Parameters Identification of the Large Inertia Rotating Component of Satellite

Xueqin Chen[1], Boyu Yang[1], Fan Wu[1*], Hongxu Wang[1], Qihan Ma[1], Chengfei Yue[2]

[1]*Research Center of the Satellite Technology, Harbin Institute of Technology, Harbin 150001, China*;
cxqhit@163.com
yoangboyu@126.com
wufanrcst@hit.edu.cn
zwwhx-hit@outlook.com
maqihanmaqihan@126.com

[2]*Institute of Space Science and Applied Technology, Harbin Institute of Technology Shenzhen, Shenzhen 518055, China*
hitychf@gmail.com

ABSTRACT

Firstly, the dynamics model with unbalance parameters of the large inertia rotating component is established. Then, based on the principle of parameter separation and decoupling, a modified two-stage exogenous Kalman filter (TSXKF) algorithm is proposed. This method works directly on a nonlinear system, estimates the centroid position, the centroid velocity, attitude angular, and attitude angular velocity, and identifies the nonlinear unknown static unbalance parameter, which is the centroid offset. Finally, the simulation results verify the effectiveness of the method.

1. INTRODUCTION

In recent years, the structure of spacecraft has shown diversity. One of the satellites is a type of rotating parts with large moments of inertia, as shown in Figure 1 (Niu, 2021). The characteristic of this kind of satellite is that the body is composed of two parts: the satellite platform and the rotating load component.

During onboard normal operation, the satellite platform maintains three-axis stability, and the rotating component moves around the satellite platform at high angular speed under the action of the control torque. When the rotating component rotates at high speed, its dynamic and static unbalances will disturb the satellite platform. During the orbit of the satellite, due to various special environments, such as temperature, magnetic field, etc., the centroid of the rotating component will deviate from the standard position, which is the static unbalance. Therefore, it is necessary to identify the static unbalance parameter while identifying the attitude information of the rotating component.

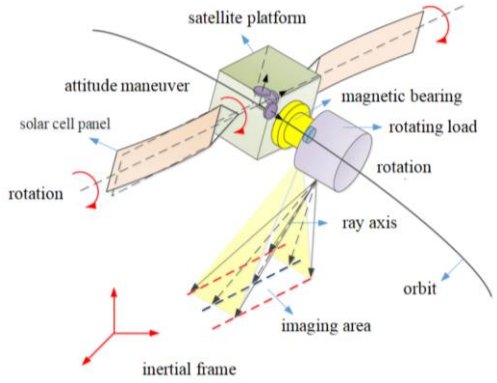

Fig. 1 Schematic diagram of satellite structure

In terms of parameter identification, the methods and applications at present are relatively mature. Parameter identification methods are not only applied to linear systems (Pan et al., 2017; Xu, 2016; Pan et al., 2018) but also to dynamic systems (Gu et al., 2019; Ma et al., 2019) and nonlinear systems (Ding et al., 2011). Parameter identification methods include particle filtering method (Ding et al., 2019), multi-information stochastic gradient method (Ding et al., 2011), etc. For the characteristics of nonlinear systems, parameter identification methods also include over-parameterized identification method (Chen et al.,2020), maximum likelihood identification method (Zhao et al., 2018), auxiliary model identification method (Ding et al., 2011; Wang et al., 2018), etc.

The parameter identification method adopted in this paper is based on the two-stage Kalman filter (TSKF) method. TSKF differs from the conventional algorithm in parameter separation and decoupling, which can reduce the amount of

calculation and improve the stability of calculation. However, for a long time, the two-stage Kalman filter is usually applied in linear systems or weak nonlinear systems. In practical application, nonlinear system accounts for a large proportion of systems. For traditional Kalman filter algorithm, there are many ways to deal with nonlinear systems: Extended Kalman filter (EKF), unscented Kalman filter (UKF) and so on. All these methods can be applied to the second stage Kalman filter to obtain an algorithm that has the advantages of both nonlinear and parameter separation.

The two-stage extended Kalman filter (TSEKF) based on EKF principle can deal with nonlinear systems (Hsieh & Chen, 1995), but Taylor's formula retaining the first order will result in large errors of the results and poor processing effect for highly nonlinear systems. The two-stage unscented Kalman filter (TSUKF) based on UKF principle has higher accuracy than TSEKF, but the accuracy and stability of sampling points sometimes have problems. Especially for low-dimensional nonlinear systems, the TSUKF has a better effect than general methods (Xu & Jing, 2008).

The filtering method used in this paper is the two-stage exogenous Kalman filter (TSXKF). TSXKF introduces a nonlinear observer on the basis of TSEKF's method, which can make up for TSEKF's shortcomings in accuracy (Chen, 2020). Taylor series expansion is performed at the observed value of the nonlinear observer to perform local linearization of the model. The observed value converges to the state value, and the error corresponding to Taylor expansion converges to zero.

In section 2, the dynamic model of the large moment of inertia rotating component is given. Section 3 introduces the modified TSXKF algorithm. Finally, simulation analysis is carried out to prove the feasibility of the algorithm.

2. DYNAMICAL MODEL

Under normal circumstances, the rotating component rotates around the satellite platform under the constraint of the 5 degrees of freedom magnetic levitation bearing. To calculate the air gap of magnetic suspension bearing, the corresponding coordinate system between satellite platform and rotating component should be established firstly, and the relative position relationship should be defined. Consider the magnetic levitation bearing rotor model shown in Fig.2 (Niu, 2021).

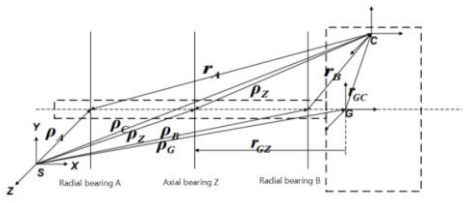

(a) Initial state

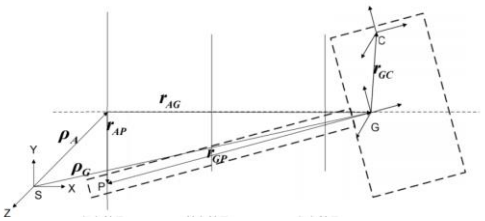

(b) Spinning state

Fig.2 Definition of position relation of magnetic bearing rotor

Three coordinates are established in Fig.2: platform coordinate S, rotating component center coordinate G, and rotating component centroid coordinate C.

Define the attitude angle of the rotating component

$$\boldsymbol{\Psi} = [\varphi \ \theta \ \psi]^{\mathrm{T}} \tag{1}$$

where, $\boldsymbol{\Psi} \in \mathbb{R}^3$ then the direction cosine matrix of coordinate G relative to the coordinate S can be written as

$$\boldsymbol{\Phi}_{gs} = \begin{bmatrix} C_\theta C_\psi & C_\theta S_\psi & -S_\theta \\ -C_\varphi S_\psi + S_\varphi S_\theta C_\psi & C_\varphi C_\psi + S_\varphi S_\theta S_\psi & S_\varphi C_\theta \\ S_\varphi S_\psi + C_\varphi S_\theta C_\psi & -S_\varphi S_\psi + C_\varphi S_\theta S_\psi & C_\varphi C_\theta \end{bmatrix} \tag{2}$$

The translational dynamic equation of the magnetic suspension rotor with the nominal centroid G as the reference point can be obtained as

$$\begin{aligned} \dot{\boldsymbol{v}}_g &= -\boldsymbol{\Phi}_{gs}^{\mathrm{T}} \\ &(\dot{\boldsymbol{\omega}} \times \boldsymbol{r}_{GC} + \boldsymbol{\omega} \times (\boldsymbol{\omega} \times \boldsymbol{r}_{GC})) + \frac{1}{m} \boldsymbol{f}_c \end{aligned} \tag{3}$$

where, $\boldsymbol{v}_g \in \mathbb{R}^3$ is the centroid velocity of the rotating component, $\boldsymbol{\omega} \in \mathbb{R}^3$ is the attitude angular velocity of the rotating component, $\boldsymbol{r}_{GC} \in \mathbb{R}^3$ is the vector from the origin center coordinate to the origin of the load centroid coordinate, and describes the centroid offset of the rotating component. m is the mass of the rotating component. $\boldsymbol{f}_A$, $\boldsymbol{f}_B$, $\boldsymbol{f}_Z$ are the forces exerted by bearings A, B and Z and

$$\boldsymbol{f}_c = \boldsymbol{f}_A + \boldsymbol{f}_B + \boldsymbol{f}_Z$$

The rotational dynamics equation of the rotating component is

$$\begin{aligned} \boldsymbol{J}\dot{\boldsymbol{\omega}} &= -\boldsymbol{\omega} \times \boldsymbol{J}\boldsymbol{\omega} - \boldsymbol{\Phi}_{gs}(\boldsymbol{\rho}_G \times \boldsymbol{f}_C) - \\ &\boldsymbol{r}_{GC} \times (\boldsymbol{\Phi}_{gs} \boldsymbol{f}_C) + \boldsymbol{\Phi}_{gs} \boldsymbol{\rho}_{AB} \times \boldsymbol{f}_B + \boldsymbol{T}_C \end{aligned} \tag{4}$$

where, $\boldsymbol{J} \in \mathbb{R}^{3\times3}$ is the moment of inertia of the rotating component. $\boldsymbol{\rho}_G \in \mathbb{R}^3$ is the centroid position, $\boldsymbol{\rho}_{\mathrm{AB}} \in \mathbb{R}^3$ is the vector pointing from the center of radial bearing A to the center of bearing B. $\boldsymbol{T}_c \in \mathbb{R}^3$ stands for the torque on the rotating component which is divided into $\boldsymbol{T}_m$ and $\boldsymbol{T}_w$; $\boldsymbol{T}_m \in \mathbb{R}^3$ stands for the combined torque of magnetic bearing on the

rotating component center of mass; $\boldsymbol{T}_w \in \mathbb{R}^3$ stands for the control torque generated by the actuators on the rotating component.

Define the system state vector of the rotating component is

$$\boldsymbol{x} = [\boldsymbol{\rho}_G^{\mathrm{T}} \ \boldsymbol{v}_g^{\mathrm{T}} \ \boldsymbol{\Psi}^{\mathrm{T}} \ \boldsymbol{\omega}^{\mathrm{T}}]^{\mathrm{T}} \tag{5}$$

Define the bias parameter

$$\boldsymbol{b} = \boldsymbol{r}_{GC}$$

The system state-space equation can be written as

$$\dot{\boldsymbol{x}} = \boldsymbol{f}(\boldsymbol{x}, \boldsymbol{b}) \tag{6}$$

where

$$\boldsymbol{f}(\boldsymbol{x}, \boldsymbol{b}) = \begin{bmatrix} \boldsymbol{v}_g \\ \boldsymbol{f}_1(\boldsymbol{x}, \boldsymbol{b}) \\ \boldsymbol{\omega} \\ \boldsymbol{f}_2(\boldsymbol{x}, \boldsymbol{b}) \end{bmatrix} \tag{7}$$

where

$$\boldsymbol{f}_1(\boldsymbol{x}, \boldsymbol{b}) = \dot{\boldsymbol{v}}_g \tag{8}$$

$$\boldsymbol{f}_2(\boldsymbol{x}, \boldsymbol{b}) = \boldsymbol{J}^{-1} \begin{Bmatrix} -\boldsymbol{\omega} \times \boldsymbol{J}\boldsymbol{\omega} - \boldsymbol{\Phi}_{gs}(\boldsymbol{\rho}_G \times \boldsymbol{f}_C) - \\ \boldsymbol{r}_{GC} \times (\boldsymbol{\Phi}_{gs} \boldsymbol{f}_C) + \boldsymbol{\Phi}_{gs} \boldsymbol{\rho}_{AB} \times \boldsymbol{f}_B + \boldsymbol{T}_C \end{Bmatrix} \tag{9}$$

3. IMPROVED TWO-STAGE EXOGENOUS KALMAN FILTER ALGORITHM

For the satellite with large inertia rotating component, the system state-space equation (6) is complex, the state variables and the bias parameter are not conducive to be estimated and identified directly. In order to avoid the complexity of the system model and the corresponding filtering algorithm increased by the conventional augmented processing methods of state variables and unknown parameters, based on the principle of parameter separation and decoupling, an improved TSXKF was proposed.

Firstly, considering the nonlinearity of the system model, the accuracy of the system model will be reduced if directly linearized and simplified. A nonlinear variable structure observer is proposed to observe the state variables and bias parameter in the system model.

Then, through the proper transformation, the system model is linearized by using the principle of deviation separation, and are estimated independently as different deviation terms in the state equation, so as to facilitate the design and extended application of the filtering algorithm.

Finally, the optimal estimation of the improved TSXKF algorithm is obtained through the unbiased estimation of state variables, the optimal estimation of bias parameter, and the coupling of state variables and unbiased estimation, as shown in Fig.3.

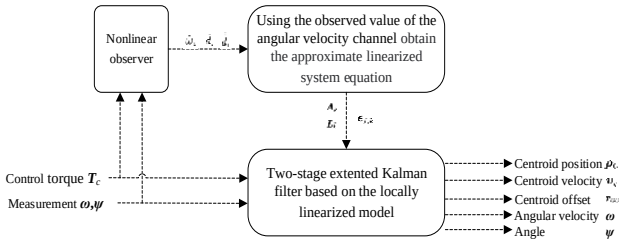

Fig.3 The improved TSXKF algorithm

3.1. Design of nonlinear variable structure observe

Design a nonlinear observer for the attitude angular velocity channel of the rotating component. The observed value of angular velocity, the bias and its first derivative can be obtained.

Locally linearize the state-space equation for the angular velocity part. The model of angular velocity channel with the unknown bias influence can be written as

$$\begin{cases} \dot{\boldsymbol{\omega}} = \boldsymbol{f}_2\left(\hat{\boldsymbol{x}}, \hat{\boldsymbol{b}}\right) + \boldsymbol{L}^{\boldsymbol{x}} \boldsymbol{b} - \boldsymbol{L}^{\boldsymbol{x}} \hat{\boldsymbol{b}} \\ \boldsymbol{y}^{\boldsymbol{\omega}} = \boldsymbol{\omega} \end{cases} \tag{10}$$

where, $\boldsymbol{L}^{x} \in \mathbb{R}^{12 \times 3}$ represents the locally linearized coefficient, where, the superscript '^' represents the estimation results of the filter algorithm.

Rearrange the formula (10)

$$\begin{cases} \dot{\boldsymbol{\omega}} = \boldsymbol{\epsilon}_{\boldsymbol{x}, \boldsymbol{b}} + \boldsymbol{d} \\ \boldsymbol{y}^{\boldsymbol{\omega}} = \boldsymbol{\omega} \end{cases} \tag{11}$$

where,

$$\boldsymbol{d} = [d_1 \ d_2 \ d_3]^{\mathrm{T}} = \boldsymbol{L}^{\boldsymbol{x}} \boldsymbol{b} \tag{12}$$

represents the unknown interference caused by the bias parameter and define

$$\boldsymbol{\epsilon}_{\boldsymbol{x}, \boldsymbol{b}} = \boldsymbol{f}_2\left(\hat{\boldsymbol{x}}, \hat{\boldsymbol{b}}\right) - \boldsymbol{L}^{\boldsymbol{x}} \hat{\boldsymbol{b}} \tag{13}$$

and

$$\boldsymbol{\omega} = [\omega_1 \ \omega_2 \ \omega_3]^{\mathrm{T}}$$

$$\boldsymbol{y}^{\omega} = [y_1^{\omega} \ y_2^{\omega} \ y_3^{\omega}]^{\mathrm{T}}$$

Then the angular velocity channel subsystem model can be written as

$$\begin{cases} \dot{\omega}_i = \epsilon_{x,bi} + d_i \\ y_i^{\omega} = \omega_i \end{cases} \quad i = 1, 2, 3 \tag{14}$$

where, $\left|\ddot{d}_i\right|<\varepsilon_i$, $\varepsilon_i>0$.

For the system model (14), the sliding mode observer can be designed as

$$\begin{aligned}
\dot{\check{\omega}}_i &= \epsilon_{x,bi}+\check{d}_i+2\mu_i^{\frac{1}{3}}\left|y_i^{\omega}-\check{\omega}_i\right|^{\frac{2}{3}}\operatorname{sgn}\left(y_i^{\omega}-\check{\omega}_i\right)\\
\dot{\check{d}}_i &= 2.12\mu_i^{\frac{2}{3}}\left|y_i^{\omega}-\check{\omega}_i\right|^{\frac{1}{3}}\operatorname{sgn}\left(y_i^{\omega}-\check{\omega}_i\right)+\dot{\check{d}}_i\\
\dot{\check{d}}_i &= 1.1\mu_i\operatorname{sgn}\left(y_i^{\omega}-\check{\omega}_i\right)
\end{aligned} \tag{15}$$

where, the superscript "ˇ" represents the output of the observer. $\mu_i>\varepsilon_i$, sgn(·) is a normal sign function, and the superscript represents the observed value of the corresponding variable.

3.2. Model preparation

Substitute the observer results as Taylor expansion points into two-stage extended Kalman filter (TSEKF) 's method.

Using the observed value $\check{\boldsymbol{\omega}}$ and $\check{\boldsymbol{d}}$ of the angular velocity channel, the observed value of the state is obtained as

$$\check{\boldsymbol{x}}=\left[\hat{\boldsymbol{\rho}}_G^{\mathrm{T}}\ \hat{\boldsymbol{v}}_g^{\mathrm{T}}\ \hat{\boldsymbol{\Psi}}^{\mathrm{T}}\ \check{\boldsymbol{\omega}}^{\mathrm{T}}\right]^{\mathrm{T}} \tag{16}$$

By discretizing the system state-space equation (6), we can obtain

$$\boldsymbol{x}_{k+1}=\boldsymbol{f}_k\left(\boldsymbol{x}_k,\boldsymbol{b}_k\right)+\boldsymbol{w}_k \tag{17}$$

where, $\boldsymbol{w}_k$ is the process noise sequence.

From (12) and (15), the Taylor series expansion of the nonlinear function $\boldsymbol{f}_k(\cdot)$ with the expansion points $\check{\boldsymbol{x}}_{k|k}$, $\check{\boldsymbol{b}}_{k|k}$ can be obtained

$$\begin{aligned}
&\boldsymbol{f}_k\left(\boldsymbol{x}_k,\boldsymbol{b}_k\right)=\boldsymbol{f}_k\left(\check{\boldsymbol{x}}_{k|k},\check{\boldsymbol{b}}_{k|k}\right)+\\
&\boldsymbol{R}_f\left(\boldsymbol{x}_k,\boldsymbol{b}_k,\check{\boldsymbol{x}}_k,\check{\boldsymbol{b}}_k\right)+\\
&\left.\frac{\partial\boldsymbol{f}_k\left(\boldsymbol{x}_k,\boldsymbol{b}_k\right)}{\partial\boldsymbol{x}_k^{\mathrm{T}}}\right|_{\substack{\boldsymbol{x}_k=\check{\boldsymbol{x}}_{k|k}\\ \boldsymbol{b}_k=\check{\boldsymbol{b}}_{k|k}}}\left(\boldsymbol{x}_k-\check{\boldsymbol{x}}_{k|k}\right)+\\
&\left.\frac{\partial\boldsymbol{f}_k\left(\boldsymbol{x}_k,\boldsymbol{b}_k\right)}{\partial\boldsymbol{b}_k^{\mathrm{T}}}\right|_{\substack{\boldsymbol{x}_k=\check{\boldsymbol{x}}_{k|k}\\ \boldsymbol{b}_k=\check{\boldsymbol{b}}_{k|k}}}\left(\boldsymbol{b}_k-\check{\boldsymbol{b}}_{k|k}\right)
\end{aligned} \tag{18}$$

Define that

$$\begin{aligned}
\boldsymbol{A}_k&=\left.\frac{\partial\boldsymbol{f}_k\left(\boldsymbol{x}_k,\boldsymbol{b}_k\right)}{\partial\boldsymbol{x}_k^{\mathrm{T}}}\right|_{\substack{\boldsymbol{x}_k=\check{\boldsymbol{x}}_{k|k}\\ \boldsymbol{b}_k=\check{\boldsymbol{b}}_{k|k}}}\\
\boldsymbol{L}_k^{x}&=\left.\frac{\partial\boldsymbol{f}_k\left(\boldsymbol{x}_k,\boldsymbol{b}_k\right)}{\partial b_k^{\mathrm{T}}}\right|_{\substack{\boldsymbol{x}_k=\check{\boldsymbol{x}}_{k|k}\\ \boldsymbol{b}_k=\check{\boldsymbol{b}}_{k|k}}}
\end{aligned} \tag{19}$$

Ignoring the remaining the remainder of Taylor expansion terms $\boldsymbol{R}_f(\cdot)$, equations (18) can be approximately abbreviated as:

$$\boldsymbol{f}_k\left(\boldsymbol{x}_k,\boldsymbol{b}_k\right)\approx\boldsymbol{A}_k\boldsymbol{x}_k+\boldsymbol{L}_k^{x}\boldsymbol{b}_k+\boldsymbol{\epsilon}_{f,k} \tag{20}$$

where

$$\boldsymbol{\epsilon}_{f,k}=\boldsymbol{f}_k\left(\check{\boldsymbol{x}}_{k|k},\check{\boldsymbol{b}}_{k|k}\right)-\boldsymbol{A}_k\check{\boldsymbol{x}}_{k|k}-\boldsymbol{L}_k^{x}\check{\boldsymbol{b}}_k \tag{21}$$

Then, we can obtain the approximate linearized system equation:

$$\begin{cases}
\boldsymbol{x}_{k+1}=\boldsymbol{A}_k\boldsymbol{x}_k+\boldsymbol{L}_k^{x}\boldsymbol{b}_k+\boldsymbol{\epsilon}_{f,k}+\boldsymbol{w}_k^{x}\\
\boldsymbol{b}_{k+1}=\boldsymbol{b}_k+\boldsymbol{w}_k^{b}\\
\boldsymbol{y}_k=\boldsymbol{C}_k\boldsymbol{x}_k+\boldsymbol{v}_k
\end{cases} \tag{22}$$

where, $\boldsymbol{w}_k^{x}$ and $\boldsymbol{w}_k^{b}$ are process noise sequences, $\boldsymbol{v}_k$ is the measurement noise sequence. The corresponding noise covariance matrices are $\boldsymbol{Q}^{x}\in\mathbb{R}^{12\times12}$, $\boldsymbol{Q}^{b}\in\mathbb{R}^{3\times3}$, and $\boldsymbol{R}\in\mathbb{R}^{6\times6}$ respectively. $\boldsymbol{C}_k\in\mathbb{R}^{6\times12}$ is the output matrix.

3.3. Filter algorithm

Combined with the exogenous signals from the nonlinear observer, a filtering algorithm is derived to estimate the state $\boldsymbol{x}$ and unknown bias parameter $\boldsymbol{b}$ of the system.

For nonlinear discrete stochastic systems (22), there is the following two-stage Kalman filter:

$$\hat{\boldsymbol{x}}_{k+1|k+1}=\tilde{\boldsymbol{x}}_{k+1|k+1}+\boldsymbol{\beta}_{k+1|k+1}\hat{\boldsymbol{b}}_{k+1|k+1} \tag{23}$$

$$\boldsymbol{P}_{k+1|k+1}^{x}=\tilde{\boldsymbol{P}}_{k+1|k+1}^{x}+\boldsymbol{\beta}_{k+1|k+1}\boldsymbol{P}_{k+1|k+1}^{b}\boldsymbol{\beta}_{k+1|k+1}^{\mathrm{T}} \tag{24}$$

where $\hat{\boldsymbol{x}}_{k+1|k+1}$ and $\boldsymbol{P}_{k+1|k+1}^{x}$ are the state optimal estimation and its estimation error covariance matrix respectively, $\tilde{\boldsymbol{x}}_{k+1|k+1}$ and $\tilde{\boldsymbol{P}}_{k+1|k+1}^{x}$ are the unbiased state estimation and its estimation error covariance matrix, respectively

The unbiased state estimator is

$$\tilde{\boldsymbol{x}}_{k+1|k+1}=\tilde{\boldsymbol{x}}_{k+1|k}+\tilde{\boldsymbol{K}}_{k+1}^{x}\tilde{\boldsymbol{\gamma}}_{k+1} \tag{25}$$

$$\tilde{\boldsymbol{P}}_{k+1|k+1}^{x}=\left(\boldsymbol{E}_n-\tilde{\boldsymbol{K}}_{k+1}^{x}\boldsymbol{C}_{k+1}\right)\tilde{\boldsymbol{P}}_{k+1|k}^{x} \tag{26}$$

$$\tilde{\boldsymbol{K}}_{k+1}^{x}=\tilde{\boldsymbol{P}}_{k+1|k}^{x}\boldsymbol{C}_{k+1}^{\mathrm{T}}\left(\tilde{\boldsymbol{G}}_{k+1}\right)^{-1} \tag{27}$$

$$\tilde{\boldsymbol{G}}_{k+1}=\boldsymbol{C}_{k+1}\tilde{\boldsymbol{P}}_{k+1|k}^{x}\boldsymbol{C}_{k+1}^{\mathrm{T}}+\boldsymbol{R} \tag{28}$$

$$\tilde{\boldsymbol{\gamma}}_{k+1}=\boldsymbol{y}_{k+1}-\boldsymbol{C}_{k+1}\tilde{\boldsymbol{x}}_{k+1|k} \tag{29}$$

$$\tilde{\boldsymbol{x}}_{k+1|k}=\boldsymbol{A}_k\tilde{\boldsymbol{x}}_{k|k}+\boldsymbol{r}_k\hat{\boldsymbol{b}}_{k|k}+\boldsymbol{\epsilon}_{f,k}-\boldsymbol{\beta}_{k+1|k}\hat{\boldsymbol{b}}_{k+1|k} \tag{30}$$

$$\tilde{\boldsymbol{P}}_{k+1|k}^{x}=\boldsymbol{A}_k\tilde{\boldsymbol{P}}_{k|k}^{x}\boldsymbol{A}_k^{\mathrm{T}}+\boldsymbol{Q}^{x}+\boldsymbol{r}_k\boldsymbol{P}_{k|k}^{b}\boldsymbol{r}_k^{\mathrm{T}}-\boldsymbol{\beta}_{k+1|k}\boldsymbol{P}_{k+1|k}^{b}\boldsymbol{\beta}_{k+1|k}^{\mathrm{T}} \tag{31}$$

where, $\hat{\boldsymbol{b}}_{k+1|k+1}$ and $\boldsymbol{P}_{k+1|k+1}^{b}$ are the unknown bias estimation and its estimation error covariance matrix respectively, and the corresponding bias estimator is

$$\hat{\boldsymbol{b}}_{k+1|k+1}=\hat{\boldsymbol{b}}_{k+1|k}+\boldsymbol{K}_{k+1}^{b}\boldsymbol{\gamma}_{k+1} \tag{32}$$

$$\boldsymbol{P}_{k+1|k+1}^{b}=(\boldsymbol{E}_p-\boldsymbol{K}_{k+1}^{b}\boldsymbol{H}_{k+1|k})\boldsymbol{P}_{k+1|k}^{b} \tag{33}$$

$$\boldsymbol{K}_{k+1}^{b}=\boldsymbol{P}_{k+1|k}^{b}\boldsymbol{H}_{k+1|k}^{\mathrm{T}}\left(\boldsymbol{H}_{k+1|k}\boldsymbol{P}_{k+1|k}^{b}\boldsymbol{H}_{k+1|k}^{\mathrm{T}}+\tilde{\boldsymbol{G}}_{k+1}\right)^{-1} \tag{34}$$

$$\boldsymbol{\gamma}_{k+1}=\tilde{\boldsymbol{\gamma}}_{k+1}-\boldsymbol{H}_{k+1|k}\hat{\boldsymbol{b}}_{k+1|k} \tag{35}$$

$$\hat{\boldsymbol{b}}_{k+1|k}=\hat{\boldsymbol{b}}_{k|k} \tag{36}$$

$$\boldsymbol{P}_{k+1|k}^{b}=\boldsymbol{P}_{k|k}^{b}+\boldsymbol{Q}^{b} \tag{37}$$

The coupling relationship between the two is

$$\boldsymbol{\beta}_{k+1|k+1}=\boldsymbol{\beta}_{k+1|k}-\tilde{\boldsymbol{K}}_{k+1}^{x}\boldsymbol{H}_{k+1|k} \tag{38}$$

$$\boldsymbol{H}_{k+1|k}=\boldsymbol{C}_{k+1}\boldsymbol{\beta}_{k+1|k} \tag{39}$$

$$\boldsymbol{\beta}_{k+1|k}=\boldsymbol{r}_k\boldsymbol{P}_{k|k}^{b}\left(\boldsymbol{P}_{k+1|k}^{b}\right)^{-1} \tag{40}$$

$$\boldsymbol{r}_k=\boldsymbol{A}_k\boldsymbol{\beta}_{k|k}+\boldsymbol{L}_k^{x} \tag{41}$$

4. SIMULATION EXPERIMENTS AND RESULTS

The corresponding simulation parameters are shown follows. The mass of the rotating component is 900kg, the moment of inertia is

$$\boldsymbol{J}=\begin{bmatrix}350 & 10 & 20\\ 10 & 300 & 30\\ 20 & 30 & 320\end{bmatrix}\mathrm{kg\ m^2}$$

The initial state is

$$\boldsymbol{x}_0=[\boldsymbol{\rho}_{G0}^{\mathrm{T}}\ \boldsymbol{v}_{g0}^{\mathrm{T}}\ \boldsymbol{\Psi}_0{}^{\mathrm{T}}\ \boldsymbol{\omega}_0{}^{\mathrm{T}}]^{\mathrm{T}}$$

Setting the desired rotation angular velocity to $\boldsymbol{\omega}_d=[10\ 0\ 0]^{\mathrm{T}}\mathrm{deg/s}$ and the initial estimation states to

$$\boldsymbol{\rho}_{G0}=[1.1\ 1.1\ 1.1]^{\mathrm{T}}\mathrm{m}$$

$$\boldsymbol{v}_{g0}=[1\ 1\ 1]^{\mathrm{T}}\mathrm{m/s}$$

$$\boldsymbol{\Psi}_0=[-57.3\ 0\ 0]^{\mathrm{T}}\mathrm{deg}$$

$$\boldsymbol{\omega}_0=[0\ 0\ 0]^{\mathrm{T}}\mathrm{deg/s}$$

The initial value of the offset of the rotating component centroid position is zero. The set values are

$$\boldsymbol{r}_{GC}=[0.01\ 0.02\ 0.03]^{\mathrm{T}}\mathrm{m}$$

$$\boldsymbol{\rho}_G=[0.5\ 0\ 0]^{\mathrm{T}}\mathrm{m}$$

The mean square errors of the corresponding noise covariance matrices are shown in Table 1.

Table 1 Simulation parameter setting

Name of parameter	Sign	Value
Mean square error of position prediction(m)	σ_ρ	1e-4
Mean square error of velocity prediction(m/s)	σ_v	1e-2
Mean square error of centroid offset(m)	σ_r	1e-2
Mean square error of angular velocity(deg/s)	σ_ω	1e-4
Mean square error of angular(deg)	σ_ψ	1e-4

The simulation results are shown in the following figures.

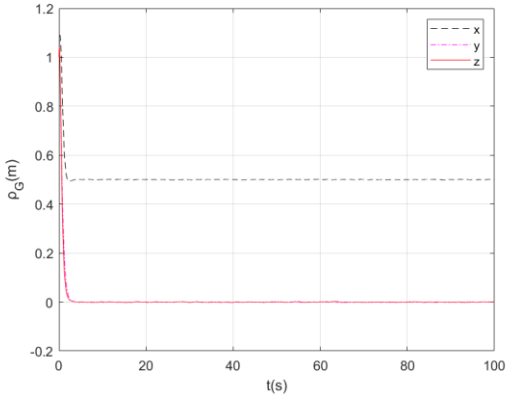

Fig.4 Centroid position estimation results

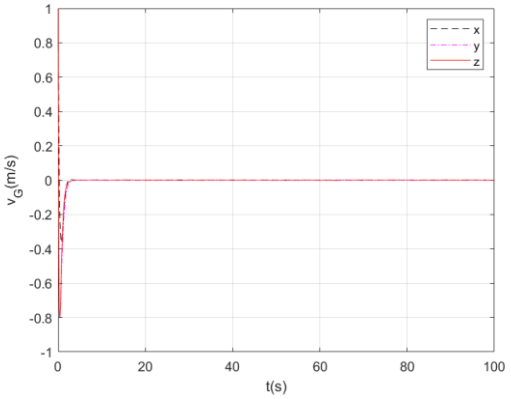

Fig.5 Centroid velocity estimation results

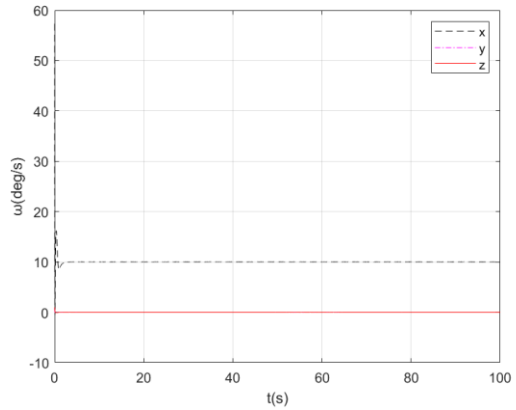

Fig.6 Attitude angular velocity estimation results

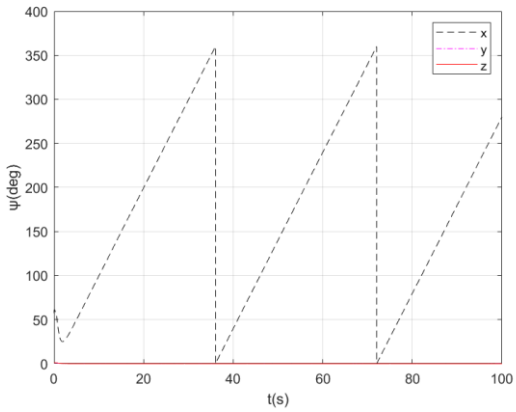

Fig.7 Attitude angle estimation results

Fig.4 is the centroid position estimation results. It can be seen from the figure that the estimation position converges to the set value rapidly in almost 5s and the estimation error is better than 8×10^{-4}m. The constant offset is 0.5m, indicating that the centroid position is affected by a static unbalance with *x*-axis.

Fig.5 is the centroid velocity estimation results. It can be seen from the figure that the estimation velocity converges to the set value rapidly in almost 5s and the estimation error is better than 2×10^{-4}m/s.

Fig.6 and Fig.7 are the attitude angular velocity estimation results and the attitude angle estimation results. The analysis of images in Fig.4~Fig.7 shows that the estimation process converges to the set value rapidly in almost 3s. The attitude angular velocity estimation error is better than 10^{-3}deg/s and the attitude angle estimation error is better than 2×10^{-4}deg.

Fig.8 is the centroid offset estimation results. It can be seen from the figure that the estimation offset converges to the set value rapidly in almost 10s and the improved TSXKF algorithm can effectively identify the centroid offset vector of the rotating component.

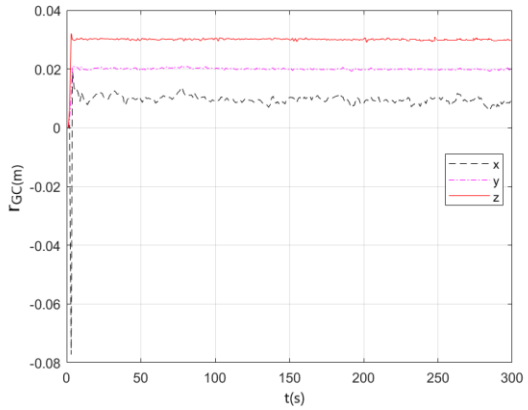

Fig.8 Centroid offset identification results

5. CONCLUSION

The improved TSXKF has been designed to solve the estimation and identification problem of the satellite rotating component, including the attitude angle, attitude angular velocity, center of mass position, center of mass velocity and the offset of the centroid position. Simulation results show that the improved TSXKF algorithm can realize the states and bias estimating accurately and rapidly.

ACKNOWLEDGEMENT

This work was supported by the National Natural Science Foundation of China [grant number: 62303138, 12372045, 11972130].

REFERENCES

Chen, M. T., Ding, F., Lin, R. M., et al. (2020). Maximum likelihood least squares-based iterative methods for output-error bilinear-parameter models with colored noises. *International Journal of Robust and Nonlinear Control*, 30 (15), 6262-6280.

Chen, X., Sun, R., Liu, M., & Song, D. (2020). Two-stage exogenous Kalman filter for time-varying fault estimation of satellite attitude control system. *Journal of the Franklin Institute*, 357, 2354.

Ding, F., Liu, X. P., & Liu, G. (2011). Identification methods for Hammerstein nonlinear systems. *Digital Signal Processing*, 21 (2), 215–238.

Ding, F., Liu, X. P., & Liu, G. (2011). Identification methods for Hammerstein nonlinear systems. *Digital Signal Processing*, 21 (2), 215–238.

Ding, F., Liu, G., Liu, X. P. (2011). Parameter estimation with scarce measurements. *Automatica*, 47 (8), 1646–1655.

Ding, J., Chen, J. Z., Lin, J. X., et al. (2019). Particle filtering based parameter estimation for systems with output-error type model structures. *Journal of the Franklin Institute*, 356 (10), 5521–5540.

Ding, J., Chen, J. Z., Lin, J. X., et al. (2019). Particle filtering-based recursive identification for controlled auto-regressive systems with quantized output. *IET Control Theory & Applications*, 13 (14), 2181–2187.

Gu, Y., Liu, J., Li, X., Chou, Y., & Ji Y. (2019). State space model identification of multirate processes with time-delay using the expectation maximization. *Journal of the Franklin Institute*, 356 (3), 1623–1639.

Gu, Y., Chou, Y., Liu, J., & Ji, Y. (2019). Moving horizon estimation for multirate systems with time-varying time-delays. *Journal of the Franklin Institute*, 356 (4), 2325–2345.

Hsieh, C. S., & Chen, F. C. (1995). Optimal solution of the two-stage Kalman estimator. *IEEE Transactions on Automatic Control*, 44 (1), 194-199.

Ma, H., Pan, J. et al. (2019). Partially-coupled least squares based iterative parameter estimation for multi-variable output-error-like autoregressive moving average systems. *IET Control Theory & Applications*, 13 (18), 3040–3051.

Niu, S. B. (2021). *Research on identification of inertia moment and centroid position for satellite with rotating payload*. Doctoral dissertation. Harbin Institute of Technology, China.

Pan, J., Jiang, X., Wan, X. K., Ding, W. (2017). A filtering based multi-innovation extended stochastic gradient algorithm for multivariable control systems. *International Journal of Control, Automation and Systems*, 15 (3), 1189–1197.

Pan, J., Li, W., Zhang, H. P. (2018). Control algorithms of magnetic suspension systems based on the improved double exponential reaching law of sliding mode control. *International Journal of Control, Automation and Systems*, 16 (6), 2878–2887.

Wang, D.Q., Li, L.W., Ji, Y., et al. (2018). Model recovery for Hammerstein systems using the auxiliary model based orthogonal matching pursuit method. *Applied Mathematical Modelling*, 54 (FEB.), 537–550.

Xu, J., Jing, Y., Dimirovski, G.M., et al. (2008). Two-stage Unscented Kalman Filter for nonlinear systems in the presence of unknown random bias. *American Control Conference*, 3530-3535.

Xu, L. (2016). The damping iterative parameter identification method for dynamical systems based on the sine signal measurement. *Signal Processing*, 120, 660–667.

Zhao, S. Y., Shmaliy, Y. S., & Ahn, C. K. (2018). Iterative maximum likelihood FIR estimation of dynamic systems with improved robustness. *IEEE/ASME Transactions on Mechatronics*, 23 (3), 1467–1476.